

# Zr-MOF@PtNPs-Based High-Recognition Colorimetric Immunochromatographic Assay Strip for Synchronous and Highly Sensitive Detection of ZEN and FB

#### Keyun Ren

Shandong University of Technology

#### Jinmiao Ma

Shandong University of Technology

#### Chunlei Yu

Shandong University of Technology

#### Xuezhen Xu

Shandong University of Technology

#### Haitao Xu

Shandong University of Technology

#### **Qingqing Yang**

yqqing@sdut.edu.cn

Shandong University of Technology

#### Research Article

Keywords: Metal-organic framework, Platinum nanoparticles, Lateral flow immunoassay, Zearalenone, Fumonisin

Posted Date: October 29th, 2025

**DOI:** https://doi.org/10.21203/rs.3.rs-7814560/v1

License: © (1) This work is licensed under a Creative Commons Attribution 4.0 International License. Read Full

License

**Additional Declarations:** No competing interests reported.

#### **Abstract**

Fusarium toxins, as significant pollutants threatening global food security, have garnered increasing attention due to their mixed contamination issues. Among them, the co-contamination rate of ZEN and FB (Total Fumonisins) in grains reaches up to 37.6%, and both exhibit synergistic toxicity, are difficult to remove, and pose serious threats to animal and human health. Therefore, developing rapid and sensitive multi-target detection technologies is of great importance. However, traditional colloidal gold-based colorimetric ICA for multi-detection suffers from drawbacks such as signal overlap and insufficient sensitivity. In this study, we synthesized a signal probe Zr-MOF@PtNPs by leveraging the high molar extinction coefficient of PtNPs and the high specific surface area of Zr-MOFs. Zr-MOF stabilizes and disperses PtNPs, enabling them to exhibit excellent colorimetric performance with superior recognition under different light backgrounds, significantly enhancing the detection sensitivity and anti-background interference capability of traditional multi-detection colorimetric ICA. In this research, a dual immunochromatographic method using Zr-MOF@PtNPs as signal labels was established for the simultaneous detection of ZEN and FB in corn, which is simple to operate and achieves detection ranges of 0.15-5 ng/mL for ZEN and 0.6–10 ng/mL for FB, with LODs of 0.27 ng/mL and 0.21 ng/mL, respectively. This improves the detection sensitivity of multi-detection colorimetric immunochromatographic assay strips for synchronous detection of ZEN and FB, providing new methodological support for the simultaneous detection of multiple mycotoxins.

#### 1 Introduction

Fusarium toxins are a collective term for various secondary metabolites produced by fungi of the Fusarium genus, which are widely distributed in nature and represent hazardous food contaminants. The toxicity mechanisms of Fusarium toxins are complex, and they have been confirmed to possess multi-system damaging properties, including hepatotoxicity, nephrotoxicity, neurotoxicity, genotoxicity, carcinogenicity, and immunosuppressive effects (Godseill et al., 2022; Qinghua, Li, Wenda, Miao, & Kamil, 2023). Fusarium toxins can easily enter the food chain through contamination, posing a major threat to human health. Within the Fusarium toxin family, ZEN and FB exhibit synergistic toxicity and commonly co-contaminate agricultural products, posing a severe threat to global food safety (Morimura et al., 2020). Notably, more than 37.6% of major grain crops such as corn and wheat, as well as their processed products (e.g., beer, feed), are co-contaminated by zearalenone (ZEN) and fumonisin (FB). Even at trace levels, they can induce oxidative stress and DNA damage, and traditional thermal processing methods cannot effectively degrade these toxins (Imourana et al., 2017; Kim et al., 2017). Moreover, traditional single-component detection methods are no longer sufficient to meet modern analytical requirements, thus urgently necessitating the development of multi-component simultaneous determination methods that are portable, sensitive, and accurate.

Traditional ICA relies on colloidal gold-based colorimetry, which offers advantages such as simple operation and low cost (Hong et al., 2022). However, most current ICA strips are designed for detecting a single type of mycotoxin, and when applied to multi-target detection, they are prone to signal overlap and insufficient sensitivity, making it difficult to meet the limit requirements for low-concentration toxins set by regulations such as those of the EU (Xing et al., 2020; Xing et al., 2015). Multi-mycotoxin ICA strips (mICA) can achieve detection of multiple targets on a single strip, shortening detection time and reducing costs. Current analytical techniques applied in mICA include colorimetric analysis, fluorescence analysis (FL), electrochemiluminescence (ECL), and photoelectrochemical (PEC) methods. Among these, colorimetry is undoubtedly the most convenient, as the output signal can be directly judged by the naked eye based on color intensity, with simple operation, low cost, visualization, and compatibility with portable instruments, making it highly suitable for on-site rapid detection (G.Panferov & JuewenLiu, 2024; Yang, Xu, Song, Huang, & Xu, 2024). However, traditional colorimetric analysis relying on AuNPs-based AuNPs-LFIA faces issues of weak signal intensity in practical applications, limiting detection sensitivity (B. Y. Sun et al., 2025; Yao et al., 2021). To

address the performance bottlenecks of traditional AuNPs-LFIA, considerable efforts have been invested in exploring novel signal-labeling nanomaterials. In recent years, the emergence of multifunctional nanomaterials has provided new ideas for enhancing ICA performance, with platinum nanoparticles (PtNPs) gaining attention due to their excellent colorimetric properties (B. Y. Sun et al., 2025). Their molar extinction coefficient is higher (several times that of AuNPs), and their inherent dark brown color forms a sharper contrast with the white background of the strip compared to the red of AuNPs, making them easier to recognize under complex backgrounds or at low concentrations, thereby improving detection sensitivity while reducing false negatives (Panferov, Wang, Zhang, & Liu, 2025). However, PtNPs are prone to aggregation due to high surface energy, limiting their applications.

Metal-organic frameworks (MOFs) are crystalline materials formed by self-assembly of metal ions or clusters with organic ligands through coordination bonds, featuring highly ordered three-dimensional porous structures (Mohanty, Kumari, Yadav, Kanoo, & Chakraborty, 2024). Their main characteristics include ultra-high specific surface area, tunable pore size, good chemical and thermal stability, and abundant surface functionalization sites, which make MOFs excel in fields such as gas storage, catalysis, drug delivery, and biosensing (Alt et al., 2022; Brij et al., 2023; Yusuf, Malek, & Kailasa, 2022). Zr<sup>4+</sup>-based metal-organic frameworks can self-assemble with antibodies through simple mixing, playing a positive role in protecting antibody activity during probe preparation. Traditional antibodies are susceptible to inactivation by environmental factors such as high temperature, extreme pH, or organic solvents, leading to decreased detection sensitivity and stability. In contrast, MOFs can encapsulate antibodies or sitespecifically conjugate them, not only maintaining the conformational integrity of antibodies but also shielding them from external interferences, ensuring their bioactivity under harsh conditions (Alt et al., 2022; Karimzadeh, Mahmoudpour, Rahimpour, & Jouyban, 2024). Their unique structural properties enable the integration of multiple signal transduction mechanisms, bridging the gap between high-sensitivity single-target assays and multiplex detection systems. Additionally, MOFs can stabilize and disperse PtNPs through their high specific surface area, preventing aggregation and enhancing colorimetric reactions in multi-target detection, suitable for on-site rapid multiindicator screening (Feng, Zhang, & Fan, 2024). These functions make MOFs ideal candidates for developing nextgeneration POC sensors that balance sensitivity, specificity, and multiplicity.

Therefore, in this study, we synthesized Zr-MOF using Zr<sup>4+</sup> as the metal center and 2-aminoterephthalic acid as the organic ligand via a one-step hydrothermal method, and utilized its high specific surface area as a dispersion carrier for PtNPs to synthesize a novel colorimetric probe Zr-MOF@PtNPs (MOF@Pt). MOF@Pt overcomes the aggregation limitation of PtNPs, maximizing their colorimetric performance. Compared to traditional colloidal gold probes, the multi-detection colorimetric immunochromatographic assay strip based on MOF@Pt exhibits excellent recognition under different light backgrounds, improving detection sensitivity and anti-background interference capability. This study demonstrates that the high-recognition colorimetric sensing platform based on MOF@Pt can achieve synchronous detection of ZEN and FB, with visual readout facilitating on-site rapid screening, simple operation, and high sensitivity, providing strong methodological support for synchronous screening of multiple mycotoxins.

#### 2 Materials and Methods

#### 2.1 Materials

ZEN monoclonal antibody was provided by the laboratory. The classic AlEgen substance tetracarboxyphenylethylene (TCPE), ZrCl<sub>4</sub>, L-ascorbic acid, and 2-aminoterephthalic acid (H<sub>2</sub>BDC-NH<sub>2</sub>) were purchased from Macklin Biotechnology Co., Ltd. Hexachloroplatinic acid hexahydrate was purchased from Shanghai Yuanye Biotechnology Co., Ltd. ZEN-BSA antigen, FB-BSA antigen, FB antibody, and goat anti-mouse IgG were purchased from Biodragon

Co., Ltd. Zearalenone (ZEN), Ochratoxin A (OTA), aflatoxin  $B_1$  (AFB<sub>1</sub>), fumonisin B (FB), T-2 toxin, Deoxynivalenol (DON) standards were purchased from Tianjin Alta Biotechnology Co., Ltd. NC membrane, gold conjugate pad, and absorbent pad were purchased from Shandong Lvdu Biotechnology Co., Ltd.

## 2.2 Instruments and Equipment

Fluorescence spectrophotometer (RF-6000) was provided by Shimadzu Corporation, Japan, and high-speed refrigerated centrifuge (Sorvall ST 16R) was supplied by Hitachi. Domestic equipment includes XYZ three-dimensional membrane spraying instrument (HM3035) and microcomputer automatic cutting machine (ZQ3055) from Shanghai Jinbiao Biotechnology Co., Ltd., ultrasonic cleaner (KQ3200E) from Kunshan Ultrasonic Instruments Co., Ltd., and three-UV analyzer (ZF-1) from Haimen Qilin Zhong Laboratory Instruments Co., Ltd. Key detection equipment includes transmission electron microscope (Tecnai G2 20, TEM) from Thermo Fisher Scientific, high-performance liquid chromatography system from Waters, and triple quadrupole tandem mass spectrometer (API QTRAP 5500) from AB SCIEX. Auxiliary instruments include 365 nm UV lamp from Shanghai Baili Biotechnology Co., Ltd., and electronic analytical balance (CAP224S) from Sartorius, Germany.

## 2.3 Preparation of Zr-MOFs, and Zr-MOF@Pt

Synthesis of Zr-MOFs: 1.86 g of  $ZrCl_4$  and 1.45 g of  $H_2BDC-NH_2$  were dissolved in DMF. The mixture was reacted in a high-pressure reactor at  $120^{\circ}C$  for 12 hours. After cooling, the solution was centrifuged at 12,000 rpm for 10 minutes and washed three times with DMF. The residue was then dried overnight under vacuum at  $60^{\circ}C$ .

Synthesis of Zr-MOF@PtNPs: 20 mg Zr-MOFs were dispersed in 20 mL ultrapure water, followed by addition of 750  $\mu$ L 40 mM  $H_2$ PtCl<sub>6</sub>·6 $H_2$ O solution, and stirring at room temperature for 30 min. Then, 3 mL 0.1 M ascorbic acid solution was injected. The mixture was ultrasonicated at 80 W for 30 min, followed by continuous stirring at 70°C for 12 h. After reaction, it was centrifuged (12000 rpm, 10 min), and the precipitate was washed three times with ultrapure water, then vacuum-dried at 85°C to obtain Zr-MOF@PtNPs (MOF@Pt) powder.

## 2.4 Preparation of Immunoprobes

MOF metal-organic frameworks have high affinity for antibodies. Therefore, MOF materials can bind to antibodies via electrostatic adsorption, maximally protecting antibody activity. The MOF@Pt suspension was mixed with 0.1 M  $K_2CO_3$ , followed by addition of ZEN or FB monoclonal antibody, and incubated at room temperature for 1 h to protect antibody activity through electrostatic adsorption. Subsequently, 100  $\mu$ L 10 mg/mL BSA was added to block unbound sites, incubated for 30 min, centrifuged at 12000 rpm for 10 min to discard the supernatant, and the precipitate was washed with 1 mg/mL BSA solution and recentrifuged. Finally, the immunoprobe was resuspended in 200  $\mu$ L solution containing 1 mg/mL BSA and 1 mg/mL Tween-20 to form MOF@Pt-Ab probe, stored at 4°C for later use.

## 2.5 Preparation of MOF@Pt-LFIA Strip

The immunochromatographic strip consists of polyvinyl chloride (PVC) board, NC membrane, sample pad, and absorbent pad.

#### Preparation of NC membrane

For the dual immunochromatographic strip, 2 mg/mL ZEN-BSA antigen ( $T_1$  line), 0.5 mg/mL FB-BSA antigen ( $T_2$  line), and 1 mg/mL secondary antibody solution (C line) were uniformly sprayed onto the NC membrane at a rate of 0.7  $\mu$ L/cm using a spraying instrument, with a line spacing of 5 mm, and dried overnight in a 37°C constant temperature incubator.

#### Preparation of sample pad

The sample pad was soaked in 100 mL blocking solution containing 0.3 g  $NaH_2PO_4$ - $2H_2O$ , 0.5 g BSA, 1.0 g PVP-K30, 2.9 g  $Na_2HPO_4$ - $12H_2O$ , 1.0 g Tween-20, and 0.25 g ethylenediaminetetraacetic acid (EDTA) for 15 min, then dried overnight in a 37°C oven.

#### Assembly of lateral flow strip

As shown in Fig. 2b, the NC membrane was tightly adhered to the PVC base plate. Then, the absorbent pad and sample pad were sequentially overlapped and adhered to the PVC base plate. The assembled immunochromatographic strip was cut into 4 mm wide strips using a cutting machine (model). Finally, the strips were placed in self-sealing bags containing desiccant and stored away from light.

#### 2.6 Detection Procedure

Under optimized conditions, corn extract was used to prepare gradient concentration standard solutions of ZEN and FB. 40  $\mu$ L mixed probe, 40  $\mu$ L 0.4% Triton-PBS, and 20  $\mu$ L standard solution were mixed in a microwell, incubated at 37°C for 5 min, and then chromatographed for 20 min. The colorimetric signals of T line and C line were recorded. The T line signal intensity of negative sample was denoted as  $T_0$ , and that of positive sample as T. The competitive inhibition rate was calculated as  $T_0$ 0. With standard concentration as the x-axis and  $T_0$ 1 as the y-axis, a competitive inhibition curve was plotted to establish the linear quantitative range and calculate the limit of detection (LOD).

ZEN and FB standards were added to corn extract at concentrations of 5, 2.5, 1.25, 0.625, and 0.315 ng/mL to determine the LOD of the POC strip detection.

With the logarithm of ZEN and FB standard concentration as the x-axis and  $B/B_0$  as the y-axis, where B represents the grayscale value of T line and B0 represents that of C line in the strip, the standard curve for detection was obtained.

The LOD value was calculated by formula (1).

$$LOD=3\delta/s$$

1

Where " $\delta$ " represents the SD of ZEN test values among 20 negative samples, and "s" represents the slope of the calibration curve.

# 2.7 Sample Pretreatment and Optimization of Loading Conditions for MOF@Pt-LFIA

## 2.7.1 Sample Pretreatment

5.0 g of corn flour was ground and extracted with 20 mL of 70% methanol/water. After centrifugation at 6000 rpm for 10 min, the supernatant was stored at 4°C. Additionally, the corn sample solution for subsequent analysis was diluted fivefold to minimize matrix interference.

# 2.7.2 Optimization of Loading Buffer

PH optimization:

The pH of negative corn samples was adjusted to 6.0, 6.5, 7.0, 7.4, and 8.0, respectively. 60  $\mu$ L of each solution was mixed with the probe in detachable microwells, reacted at 37°C for 5 min, and then added to the strip. After 20 min reaction, the T line signal values were recorded. Under the same conditions, ZEN and FB standards were added to the above solutions for competitive inhibition experiments. The T line colorimetric signal intensity under negative conditions was denoted as  $T_0$ , and under positive conditions as T. The competitive inhibition rate was defined as  $T_0$ , and  $T_0$  are influence of solution pH on strip detection performance was evaluated by competitive inhibition rate and T line colorimetric signal intensity of negative samples.

## **Optimization of methanol content:**

Under the optimal pH, negative corn sample mixed dilutions with methanol contents of 0, 5%, 10%, 20%, and 50% were accurately prepared for strip detection. Specific steps were as above. The influence of solution methanol content on strip detection performance was evaluated by competitive inhibition rate and T line colorimetric signal intensity of negative samples.

#### **Optimization of NaCl content:**

Under the optimal pH and methanol dosage, negative corn sample mixed dilutions with NaCl contents of 0 mM, 10 mM, 50 mM, 100 mM, and 200 mM were accurately prepared for strip detection. Specific steps were as above. The influence of solution NaCl content on strip detection performance was evaluated by competitive inhibition rate and T line colorimetric signal intensity of negative samples.

# 2.8 Establishment of Standard Curves for Detection of ZEN and FB in Corn Samples by MOF@Pt-LFIA

Under optimal experimental conditions, ZEN and FB standards were added to corn extract to prepare gradient concentration standard solutions. 40  $\mu$ L mixed probe, 40  $\mu$ L 0.4% Triton-PBS, and 20  $\mu$ L of the above ZEN or FB standard solution were added to detachable microwells and mixed thoroughly. The mixture was incubated at 37°C for 5 min, inserted into the strip for chromatography for 20 min, and the colorimetric signal intensities of T line and C line were recorded. The T line colorimetric signal intensity under negative conditions was denoted as  $T_0$ , and under positive conditions as T. The competitive inhibition rate was defined as  $T_0$ 0. With standard concentration as the x-axis and  $T_0$ 0 as the y-axis, a competitive inhibition curve was plotted to determine the linear quantitative range and calculate LOD.

# 2.9 Performance Evaluation of MOF@Pt-LFIA

## 2.9.1 Specificity Evaluation

The colorimetric immunochromatographic strip established in this study was used to detect four mycotoxins: AFB<sub>1</sub>, T-2, OTA, and DON, with blank samples being unmarked buffer. The specificity of the method for ZEN and FB detection was evaluated by the impact of the four mycotoxins on T line colorimetric signal intensity.

## 2.9.2 Accuracy and Precision Evaluation

ZEN standards at 2.5, 5, 10 ng/mL and FB standards at 5, 10, 50 ng/mL were added to negative corn samples, and detected using the same batch of strips as those for drawing the standard curve. Intra-batch and inter-batch

experiments were performed on the above samples to evaluate the accuracy and precision of the strips. The accuracy and precision of AIE-LFIA were evaluated by calculating the average spiked recovery rate and coefficient of variation. Intra-batch experiments were detected three times within one day, and inter-batch experiments were detected once daily for three consecutive days, with three parallels set for each concentration.

#### 3 Results and Discussion

## 3.1 Synthesis and Characterization of MOF and MOF-Pt

As shown in Fig. 2a, Zr-MOFs were synthesized via a one-step hydrothermal method, and PtNPs were deposited in situ on the surface of Zr-MOFs to prepare Zr-MOF@Pt. As depicted in Fig. 1A, Zr-MOFs exhibit irregular cubic shapes. Compared to Zr-MOFs, the morphology of Zr-MOF@Pt remains largely unchanged, presenting an irregular cubic structure (Fig. 1b). The TEM image (Fig. 1c) clearly shows PtNPs with diameters of 3–5 nm uniformly deposited on the surface of Zr-MOFs. EDS elemental analysis of MOF@Pt (Fig. 1d) reveals the uniform distribution of C, N, O, Pt, and Zr elements, which roughly constitute the overall structure of MOF@Pt. DLS measurements indicate that the average hydrodynamic diameter of MOF@Pt is 185.4 nm. Notably, MOF@Pt itself possesses a relatively low surface charge characteristic, while after conjugation with antibodies, the zeta potential shifts from – 22.6 mV to -16.47 mV and – 15.23 mV (Fig. 1e, Fig. 1f), indicating that antibody coupling alters the potential and confirms successful conjugation.

# 3.2 Working Principle of MOF@Pt-LFIA

The detection principle of the colorimetric dual immunochromatographic assay strip constructed in this study is illustrated in Fig. 2b and c. It relies on the competitive binding kinetics between ZEN, FB present in the sample, the MOF-Pt-mAb probe, and the mycotoxin-BSA conjugates immobilized on the NC membrane (Xu et al., 2021). The process begins by applying the test solution to the sample pad, which migrates laterally to the absorbent pad via capillary action. When the sample contains no target analytes, the probes MOF-Pt-AbZEN and MOF-Pt-AbFB specifically bind to the  $T_1$  line (ZEN-BSA) and  $T_2$  line (FB-BSA), respectively, forming visible detection bands; they also bind to the secondary antibody on the C line for quality control visualization. In contrast, when ZEN and FB analytes are present, the ZEN and FB standards compete with the antigens for binding to the antibodies on the probes, significantly reducing the capture efficiency of probes 1 and 2 on the T lines, resulting in T<sub>1</sub> and T<sub>2</sub> line color intensities that are negatively correlated with the target concentrations. Specifically, when only ZEN is present, the binding of probe 1 to the T<sub>1</sub> line is inhibited, while probe 2 develops normally on the T<sub>2</sub> line; conversely, when FB is present alone, it selectively inhibits color development on the T2 line. The quality control zone C line consistently maintains stable color development, validating the effectiveness of the detection system. During the detection process, due to the dark brown color labeling of Zr-MOF@Pt, MOF@Pt-LFIA exhibits high recognition under different light backgrounds (Fig. 2b), demonstrating superior anti-background interference capability compared to traditional colloidal gold-based colorimetry.

# 3.3 Optimization of MOF@Pt Antibody Conjugation Conditions

Due to their excellent specific surface area, MOFs are exceptionally well-suited for antibody loading (Deng et al., 2010; Farha et al., 2012). Therefore, we selected electrostatic adsorption—a method causing minimal damage to antibody properties—to conjugate MOF@Pt with antibodies, thereby preparing immunolabeled probes (X. Sun, Zhao, Tang, Jun, & S, 2005). The amount of  $K_2CO_3$  affects the conjugation pH, ionic strength, activity protection, and enhancement of MOF@Pt surface functionalization, which are crucial for antibody conjugation (Javdani, Shahrokh, &

Ahad, 2023; Qinghua et al., 2023; Yujia et al., 2020). Additionally, the antibody amount influences the conjugation efficiency and experimental cost; insufficient antibody leads to increased uncoupled MOF@Pt, reducing T line color development, while excessive antibody introduces steric hindrance, impeding the binding of antibodies and artificial antigens on the T line, and increases costs.

Thus, this experiment optimized the antibody conjugation conditions by investigating the effects of different  $K_2CO_3$  amounts and antibody labeling amounts on the T line colorimetric signal intensity and positive inhibition rate of the strip. As shown in Fig. 3a and c, at low  $K_2CO_3$  levels, the conjugation of ZEN-Ab and FB-Ab with MOF@Pt resulted in higher T line colorimetric signal intensity and positive inhibition rate on the strip. As the  $K_2CO_3$  amount increased, the colorimetric signal intensity and positive inhibition rate began to decrease. Meanwhile, as the ZEN-Ab labeling amount increased, the T line colorimetric signal intensity and positive inhibition rate improved (Fig. 3b). However, for FB-Ab, the optimal effect was achieved at a labeling amount of 4  $\mu$ L (Fig. 3d). Therefore, we ultimately selected 6  $\mu$ L (13.8 mg/mL)  $K_2CO_3$  and 2  $\mu$ L (10.3 mg/mL) antibody for ZEN conjugation with MOF@Pt, and 6  $\mu$ L (13.8 mg/mL)  $K_2CO_3$  and 4  $\mu$ L (5.8 mg/mL) antibody for FB conjugation with MOF@Pt.

## 3.4 Optimization of MOF@Pt-LFIA

## 3.4.1 Probe Amount and Coating Antigen Concentration

In the MOF@Pt-LFIA system, the probe amount determines the equilibrium point of competitive binding; excessive probe may lead to increased non-specific binding and elevated background signals, thereby reducing specificity, while insufficient probe results in inadequate signal intensity, affecting the limit of detection and visualization (Y. N. Sun et al., 2021). The coating antigen concentration influences the capture efficiency and competition intensity of the probe on the T line: overly high concentrations may cause saturated binding, generating non-specific signals or false positives; overly low concentrations lead to insufficient competition, weakening signals and reducing sensitivity (Shao et al., 2022).

Therefore, we ensured a stable negative correlation between the color intensities of  $T_1$  and  $T_2$  lines and the concentrations of targets (such as ZEN and FB) by optimizing the probe amount and coating antigen concentration. The optimal combination was determined based on the T line colorimetric signal intensity and positive inhibition rate of the strip. As shown in Tables 1 and 2, the highest T line colorimetric signal intensity and positive inhibition rate were achieved when the MOF@Pt-AbZEN probe amount was 20  $\mu$ L and the  $T_1$  line ZEN-BSA antigen coating concentration was 2 mg/mL; for MOF@Pt-AbFB, the probe amount was 20  $\mu$ L and the  $T_2$  line FB-BSA antigen coating concentration was 0.5 mg/mL.

 $\label{thm:continuous} Table~1$  Optimization of ZEN-BSA Coating Concentration and Probe Amount on T  $_{\rm 1}$  Line

No.	Probe Amount (µL)	ZEN-BSA Concentration (mg/mL)	T Line Colorimetric Signal Intensity (Negative)	T/C (Negative)	Inhibition Rate (%)
1	20	0.5	10357 ± 1050	0.66 ± 0.05	74.36
2	20	1	25024 ± 2365	1.05 ± 0.17	62.25
3	20	2	22905 ± 3247	1.42 ± 0.15	85.58
4	25	0.5	19162 ± 1536	0.96 ± 0.09	72.57
5	25	1	21750 ± 2582	1.32 ± 0.25	85.68
6	25	2	24658 ± 1347	1.28 ± 0.12	76.89
7	33	0.5	19624 ± 3127	0.78 ± 0.13	71.45
8	33	1	22856 ± 2878	1.16 ± 0.20	64.25
9	33	2	25109 ± 2758	0.97 ± 0.14	67.49

Table 2
Optimization of FB-BSA Coating Concentration and Probe Amount on T<sub>2</sub> Line

No.	Probe Amount (µL)	FB-BSA Concentration (mg/mL)	T Line Colorimetric Signal Intensity (Negative)	T/C (Negative)	Inhibition Rate (%)
1	20	0.25	6908 ± 536	$0.60 \pm 0.06$	59.03
2	20	0.5	24750 ± 1062	1.23 ± 0.12	84.76
3	20	1	27905 ± 890	1.32 ± 0.05	68.54
4	25	0.25	13685 ± 1536	0.86 ± 0.11	74.16
5	25	0.5	21750 ± 2336	0.96 ± 0.02	63.25
6	25	1	26658 ± 2604	1.07 ± 0.13	66.35
7	33	0.25	16055 ± 2357	1.25 ± 0.18	67.13
8	33	0.5	21856 ± 878	1.22 ± 0.20	74.29
9	33	1	26109 ± 278	0.96 ± 0.18	70.64

## 3.4.2 Reaction Time

To determine the optimal immune reaction time for MOF@Pt-LFIA, the kinetic process of the strip's immune reaction was plotted by observing the relationship between the  $T_1$  and  $T_2$  line colorimetric signal intensity values and time within 25 min. As shown in Fig. 4a and b, the values of the dual immunochromatographic assay strip remained essentially unchanged after 20 min of immune reaction; therefore, 20 min after inserting the strip was selected as the optimal chromatography time.

# 3.4.3 Buffer Solution pH

The buffer solution pH affects the stability and binding affinity of antibody-antigen complexes. Due to the fragility of antibodies, high acidity, alkalinity, or organic solvents can disrupt antibody structure, impacting antigen-antibody

interactions and thus the strip's sensitivity. We evaluated the effects on strip sensitivity and stability by measuring different pH values (6-8). As shown in Fig. 4c and f, when the buffer pH was 7.0, the strip's inhibition rate was highest, and the corresponding T/C value was also maximal, yielding the best effect.

#### 3.4.4 Buffer Solution NaCl Concentration

The buffer solution NaCl concentration influences electrolyte balance and protein interactions: high NaCl concentrations may shield electrostatic attractions, leading to weakened binding or poor flow; low concentrations may increase non-specific adsorption, elevating background noise (Hnasko, Jackson, Lin, Haff, & McGarvey, 2021). As shown in Fig. 4d and g, when the NaCl concentration was 10 mM, the strip's competitive inhibition rate and T/C value reached the maximum.

### 3.4.5 Buffer Solution Methanol Concentration

Inappropriate buffer solution methanol concentrations can interfere with immune binding: high methanol concentrations may reduce antibody activity and sensitivity; low concentrations may affect toxin extraction from samples (Zhao et al., 2021). As shown in Fig. 4e and h, the strip's inhibition rate varied with methanol concentration changes, reaching the highest when the methanol concentration was 10%, indicating that the methanol concentration in the buffer should not exceed 10%.

## 3.5 Evaluation of MOF@Pt-LFIA

# 3.5.1 Specificity

To evaluate the specificity of MOF@Pt-LFIA, we used MOF@Pt-LFIA to detect other common toxins in corn, including AFB<sub>1</sub>, T-2, OTA, and DON. As shown in Fig. 5, when detecting the corresponding target toxins, the colorimetric signal intensity of the corresponding T line weakened or even disappeared, whereas when detecting AFB<sub>1</sub>, T-2, OTA, and DON, the colorimetric signal intensities of the T and C lines remained essentially unchanged. The above results indicate that the established MOF@Pt-LFIA possesses good specificity for ZEN and FB.

# 3.5.2 Accuracy and Precision Evaluation

The accuracy and precision of the multi-dual immunochromatographic method developed in this study were evaluated by analyzing corn artificially contaminated with ZEN at concentrations of 2.5, 5, and 10 ng/mL and FB at concentrations of 5, 10, and 15 ng/mL. The results are shown in Table 3. The method's intra-batch and inter-batch average spiked recovery rates for ZEN in corn samples were 97.74%-112.24%, with coefficients of variation of 1.05%-8.24%; for FB, the intra-batch and inter-batch average spiked recovery rates were 93.43%-107.94%, with coefficients of variation of 3.19%-11.07%. The above research results demonstrate that the dual immunochromatographic assay strip based on MOF@Pt exhibits good accuracy and precision.

Table 3
Precision and Accuracy of Dual Immunoassay for Detection of ZEN and FB in Corn

(ng/mL) Detected Recovery CV Detected Recovery C Concentration Rate (%) (%) Concentration Rate (%) (° (ng/mL) (ng/mL)	Sample	Fusarium Toxin	Spiked Concentration (ng/mL)	Intra-batch Experiment <sup>a</sup>			Inter-batch Experiment <sup>b</sup>		
Corn ZEN 10 9.84 98.40 6.41 9.68 96.8 3				Concentration			Concentration		CV (%)
	Corn	ZEN	10	9.84	98.40	6.41	9.68	96.8	3.26
5 4.82 96.40 3.72 5.14 102.8 8			5	4.82	96.40	3.72	5.14	102.8	8.24
2.5 2.88 115.20 5.61 2.36 94.4 5			2.5	2.88	115.20	5.61	2.36	94.4	5.25
FB 15 15.86 105.73 5.51 16.32 108.8 1		FB	15	15.86	105.73	5.51	16.32	108.8	1.38
10 8.62 86.2 1.68 9.58 95.8 2			10	8.62	86.2	1.68	9.58	95.8	2.21
5 5.87 117.4 8.25 5.24 104.8 7			5	5.87	117.4	8.25	5.24	104.8	7.96

a Each spiked concentration was measured in triplicate, and the average was taken.

# 3.6 Real Sample Detection by MOF@Pt-LFIA

Based on the optimal reaction parameters, this study systematically investigated the capability of the MOF@Pt-based dual immunochromatographic system for simultaneous detection of ZEN and FB in corn. By constructing gradient dilution series of ZEN and FB toxin standards and combining the dose-response relationship between colorimetric signal intensity and target concentration, the sensor's synergistic detection sensitivity and specificity for dual targets were verified. As shown in the physical images in Fig. 6a and b, the spiked final concentrations of ZEN in corn samples were 0.03-10 ng/mL, and for FB, 0.03-10 ng/mL. As the concentrations of ZEN and FB increased, the colorimetric signal intensity of the corresponding T lines on the strip decreased or even disappeared, because the standards in the test solution competed with the antigens coated on the T lines for binding to the immunodetection probes, thereby inhibiting probe capture on the T lines. Competitive inhibition curves were plotted with the spiked concentrations of ZEN or FB as the x-axis and T/T<sub>0</sub> as the y-axis. As shown in Fig. 6c and d, when the ZEN concentration was in the range of 0.15-5 ng/mL, T/T<sub>0</sub> exhibited a good linear correlation with the logarithmic value of ZEN concentration, with the regression equation for ZEN detection in corn matrix being Y = -0.59784 X + 0.61386, R<sup>2</sup> = 0.99849. When the FB concentration was in the range of 0.6–10 ng/mL,  $T/T_0$  showed a good linear correlation with the logarithmic value of FB concentration, with the regression equation for FB detection in corn matrix being Y = -0.88481 X + 0.89959,  $R^2 = 0.98956$ . Negative samples were measured 20 times to obtain the standard deviation (SD) of negative samples. Calculations revealed that the LOD of MOF@Pt-LFIA for ZEN in corn samples was 0.27 ng/mL, and for FB, 0.21 ng/mL. Compared with other studies in Table 4, the MOF@Pt-LFIA constructed in this paper achieved a lower detection limit in multi-detection immunochromatographic strips for FB, and most current detections for fumonisins focus on FB<sub>1</sub>, whereas this study targets FB with broader applicability. Additionally, the detection limit of the MOF@Pt-LFIA constructed in this paper for ZEN in multi-detection colorimetric immunochromatographic strips also achieved satisfactory results.

#### 4. Conclusion

In response to the urgency of innovating rapid multi-target detection technologies for mycotoxins and the drawbacks of traditional colloidal gold-based colorimetric ICA in multi-detection, such as signal overlap and insufficient

b One experiment was completed daily for three consecutive days.

sensitivity, this study synthesized MOF@Pt as a novel signal probe by dispersing PtNPs with Zr-MOFs. MOF@Pt utilizes the high specific surface area of Zr-MOFs to successfully compensate for the aggregation defect of PtNPs, enabling them to exhibit excellent colorimetric performance and recognition under different light backgrounds. Based on MOF@Pt, a high-recognition dual colorimetric immunoassay method was established for detecting ZEN and FB in corn matrix. Through condition optimization, the optimal usage conditions for MOF@Pt-LFIA were obtained. Under optimal conditions, MOF@Pt-LFIA successfully achieved rapid detection of ZEN and FB, two Fusarium toxins, in corn matrix, with detection ranges of 0.15-5 ng/mL and 0.6–10 ng/mL, and LODs of 0.27 ng/mL and 0.21 ng/mL, respectively, improving the detection sensitivity of multi-detection colorimetric immunochromatographic assay strips for synchronous detection of ZEN and FB. This method showed no obvious cross-reactivity with four other common mycotoxins, demonstrating good specificity. Furthermore, the developed method exhibited high precision, sensitivity, and satisfactory recovery rates when applied to real samples. The above results indicate that the dual immunochromatographic assay strip constructed in this study can be used for highly sensitive simultaneous detection of multiple mycotoxins in corn samples, suitable for portable and rapid on-site screening in food safety and other point-of-care testing applications.

#### **Declarations**

## **Declaration of competing interest:**

The authors declare that they have no known competing financial interests or personal relationships that could have appeared to influence the work reported in this paper.

## **Contributions:**

Keyun Ren: Writing – original draft, Writing – review & editing, Formal analysis. Jinmiao Ma: Writing – review & editing, Data curation, Methodology. Chunlei Yu: Investigation, Validation. Xuezhen Xu: Formal analysis, Methodology. Haitao Xu: Conceptualization, Data curation, Methodology. Qingqing Yang: Funding acquisition, Project administration, Resources, Conceptualization. All authors reviewed the manuscript.

#### **Author Contribution**

Keyun Ren: Writing – original draft, Writing – review & editing, Formal analysis. Jinmiao Ma: Writing – review & editing, Data curation, Methodology. Chunlei Yu: Investigation, Validation. Xuezhen Xu: Formal analysis, Methodology. Haitao Xu: Conceptualization, Data curation, Methodology. Qingqing Yang: Funding acquisition, Project administration, Resources, Conceptualization. All authors reviewed the manuscript.

## **Acknowledgment:**

This work was supported by the Natural Science Foundation of Shandong Province (ZR2025MS367).

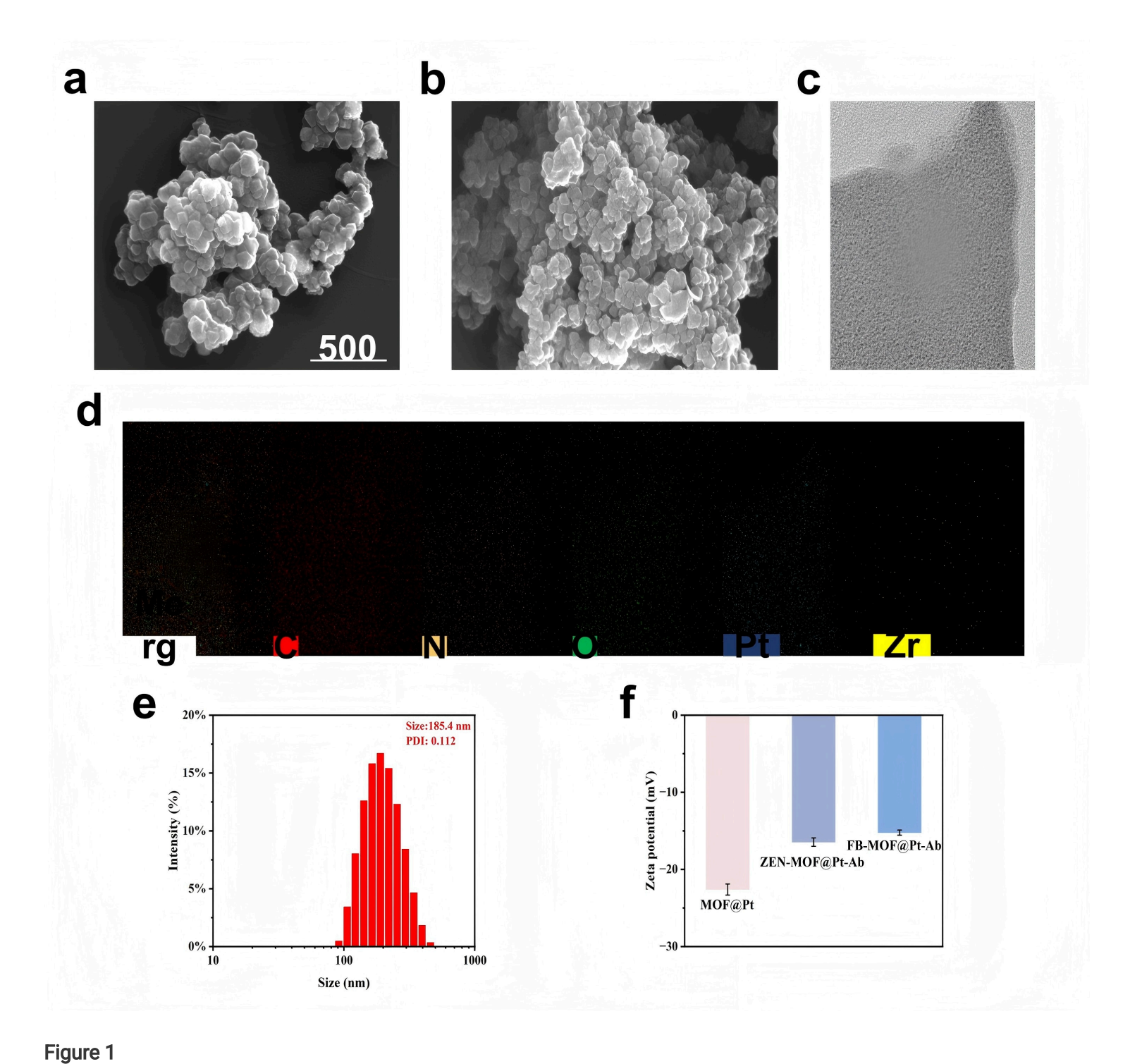
#### References

1. Alt K, Carraro F, Jap E, Linares-Moreau M, Riccò R, Righetto M, Bogar M, Amenitsch H, Hashad RA, Doonan C, Hagemeyer CE, Falcaro P (2022) Self-Assembly of Oriented Antibody-Decorated Metal-Organic Framework

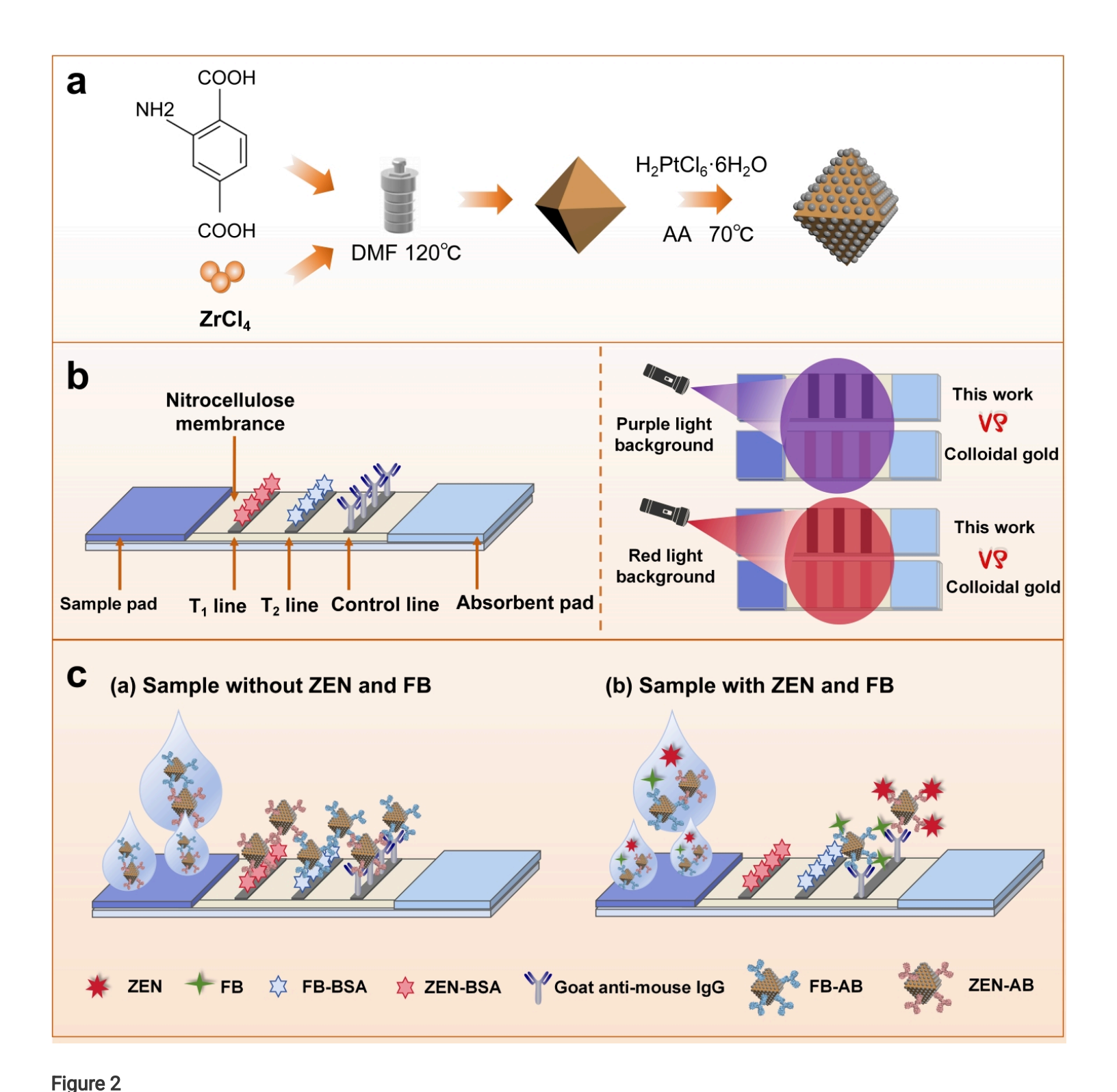
- Nanocrystals for Active-Targeting Applications. Advanced Materials, 34 (21)
- 2. Brij M, Diksha D, Virender, Mehak, Priyanka, Qiming S, Masood J, Gurjaspreet S, Neera R (2023) Metal-organic frameworks (MOFs) structural properties and electrochemical detection capability for cancer biomarkers. Microchem J, 193
- 3. Deng H, Doonan CJ, Furukawa H, Ferreira RB, Towne J, Knobler CB, Wang B, Yaghi OM (2010) Multiple Functional Groups of Varying Ratios in Metal-Organic Frameworks. Science 327(5967):846–850
- 4. Farha OK, Eryazici I, Jeong NC, Hauser BG, Wilmer CE, Sarjeant AA, Snurr RQ, Nguyen ST, Yazaydin A, Hupp JT (2012) Metal-Organic Framework Materials with Ultrahigh Surface Areas: Is the Sky the Limit? J Am Chem Soc 134(36):15016–15021
- 5. Feng L, Zhang M, Fan Z (2024) Current trends in colorimetric biosensors using nanozymes for detecting biotoxins (bacterial food toxins, mycotoxins, and marine toxins). *Analytical methods: advancing methods and applications*
- 6. Panferov G, V., JuewenLiu (2024) Optical and Catalytic Properties of Nanozymes for Colorimetric Biosensors: Advantages, Limitations, and Perspectives. Adv Opt Mater 12(30):2401318–2401318
- 7. Godseill AC, Nyakundi OE, Sarah N, Akinyi OG, Josiah El, Hannington T, U., O. C., K., U. A., O., A. A.,R., O. C. O (2022) Mycotoxins' Toxicological Mechanisms Involving Humans, Livestock and Their Associated Health Concerns: A Review. Toxins 14(3):167–167
- 8. Hnasko RM, Jackson ES, Lin AV, Haff RP, McGarvey JA (2021) A rapid and sensitive lateral flow immunoassay (LFIA) for the detection of gluten in foods. Food Chem, *355*
- 9. Hong, S., Yuping, W., Xiaosheng, W., Yu, Z., Jingwen, L., Tingting, C., Han, S., Haifeng, C., Kailun, H., Guangpeng, H., Xu, C., Guoqiang, L., & Meihong, D. (2022). Hapten designs based on aldicarb for the development of a colloidal gold immunochromatographic quantitative test strip. *Frontiers in Nutrition*, *9*, 976284–976284
- 10. Imourana A-K, Gerd S, Ionelia T, Daniela M, Olivier P, Paule OI (2017) Mycotoxins co-contamination: Methodological aspects and biological relevance of combined toxicity studies. Crit Rev Food Sci Nutr 57(16):3489–3507
- 11. Javdani EH, Shahrokh S, Ahad G (2023) Improved structure of Zr-BTC metal organic framework using NH2 to enhance CO2 adsorption performance. Sci Rep 13(1):17700–17700
- 12. Karimzadeh Z, Mahmoudpour M, Rahimpour E, Jouyban A (2024) Recent advancements in the specific determination of carcinoembryonic antigens using MOF-based immunosensors. RSC Adv 14(14):9571–9586
- 13. Kim D-H, Hong S-Y, Kang JW, Cho SM, Lee KR, An TK, Lee C, Chung SH (2017) Simultaneous Determination of Multi-Mycotoxins in Cereal Grains Collected from South Korea by LC/MS/MS. Toxins 9(3):106–106
- 14. Mohanty B, Kumari S, Yadav P, Kanoo P, Chakraborty A (2024) Metal-organic frameworks (MOFs) and MOF composites based biosensors. Coord Chem Rev 519:216102—216102
- 15. Morimura H, Ito M, Yoshida S, Koitabashi M, Tsushima S, Camagna M, Chiba S, Takemoto D, Kawakita K, Sato I (2020) In Vitro Assessment of Biocontrol Effects on Fusarium Head Blight and Deoxynivalenol (DON) Accumulation by DON-Degrading Bacteria. Toxins 12(6):399
- 16. Panferov VG, Wang SH, Zhang WJ, Liu JW (2025) Au@Ag, Au@Pd, Au@Pt and Au@Ir Nanoparticles as Colorimetric and Peroxidase-Like Labels for Lateral Flow Assays. Acs Appl Nano Mater 8(36):17754–17767
- 17. Qinghua W, Li Y, Wenda W, Miao L, Kamil K (2023) Mycotoxins: Emerging toxic mechanisms, and unanswered research questions. Food Chem toxicology: Int J published Br Industrial Biol Res Association 174:113673–113673

- 18. Shao SB, Shang WH, Bai YC, Dou LN, Zhang SX, Shen JZ, Wang ZH, Wen K (2022) Development of a Highly Sensitive and Specific ic-ELISA and Lateral Flow Immunoassay for Diacetoxyscirpenol. Foods 11:11
- 19. Sun BY, Panferov V, Guo XW, Xiong JC, Zhang S, Qin LQ, Yin CC, Wang XM, Liu CJ, Han K, Wang SH, Jiang HY (2025) A novel triple-signal biosensor based on ZrFe-MOF@PtNPs for ultrasensitive aflatoxins detection. Biosens Bioelectron, *267*
- 20. Sun X, Zhao X, Tang J, Jun Z, S CF (2005) Preparation of gold-labeled antibody probe and its use in immunochromatography assay for detection of aflatoxin B1. Int J Food Microbiol 99(2):185–194
- 21. Sun YN, Yang SZ, Yang JF, Hu XF, Wei Q, Wang Y, Xing YR, Chen LL, Chen XX, Deng RG, Zhang GP (2021) An accurate and amplifying competitive lateral flow immunoassay for the sensitive detection of haptens. Food Agricultural Immunol 32(1):766–777
- 22. Xing C, Dong X, Xu T, Yuan J, Yan W, Sui X, Zhao X (2020) Analysis of multiple mycotoxins-contaminated wheat by a smart analysis platform. Anal Biochem 610:113928–113928
- 23. Xing C, Liu L, Song S, Feng M, Kuang H, Xu C (2015) Ultrasensitive immunochromatographic assay for the simultaneous detection of five chemicals in drinking water. Biosens Bioelectron 66:445–453
- 24. Yang L, Xu X, Song Y, Huang J, Xu H (2024) Research progress of nanozymes in colorimetric biosensing: Classification, activity and application. Chem Eng J 487:150612
- 25. Yao XL, Wang ZH, Zhao M, Liu SJ, Su LH, Dou LN, Li T, Wang JL, Zhang DH (2021) Graphite-like carbon nitride-laden gold nanoparticles as signal amplification label for highly sensitive lateral flow immunoassay of  $17\beta$ -estradiol. Food Chem, 347
- 26. Yujia S, Liwei Z, Yu Y, Xu Q, Ting F, Xiaowei L, Zunyi Y, He Y, Cheng C, Weihong T (2020) Metal-Organic Framework Nanocarriers for Drug Delivery in Biomedical Applications. Nano-Micro Lett 12(1):103-103
- 27. Yusuf VF, Malek NI, Kailasa SK (2022) Review on Metal-Organic Framework Classification, Synthetic Approaches, and Influencing Factors: Applications in Energy, Drug Delivery, and Wastewater Treatment. Acs Omega 7(49):44507–44531
- 28. Zhao S, Bu T, He KY, Bai FE, Zhang M, Tian YM, Sun XY, Wang X, Hui ZS, Wang L (2021) A novel  $\alpha$ -Fe2O3 nanocubes-based multiplex immunochromatographic assay for simultaneous detection of deoxynivalenol and aflatoxin B1 in food samples. Food Control, 123

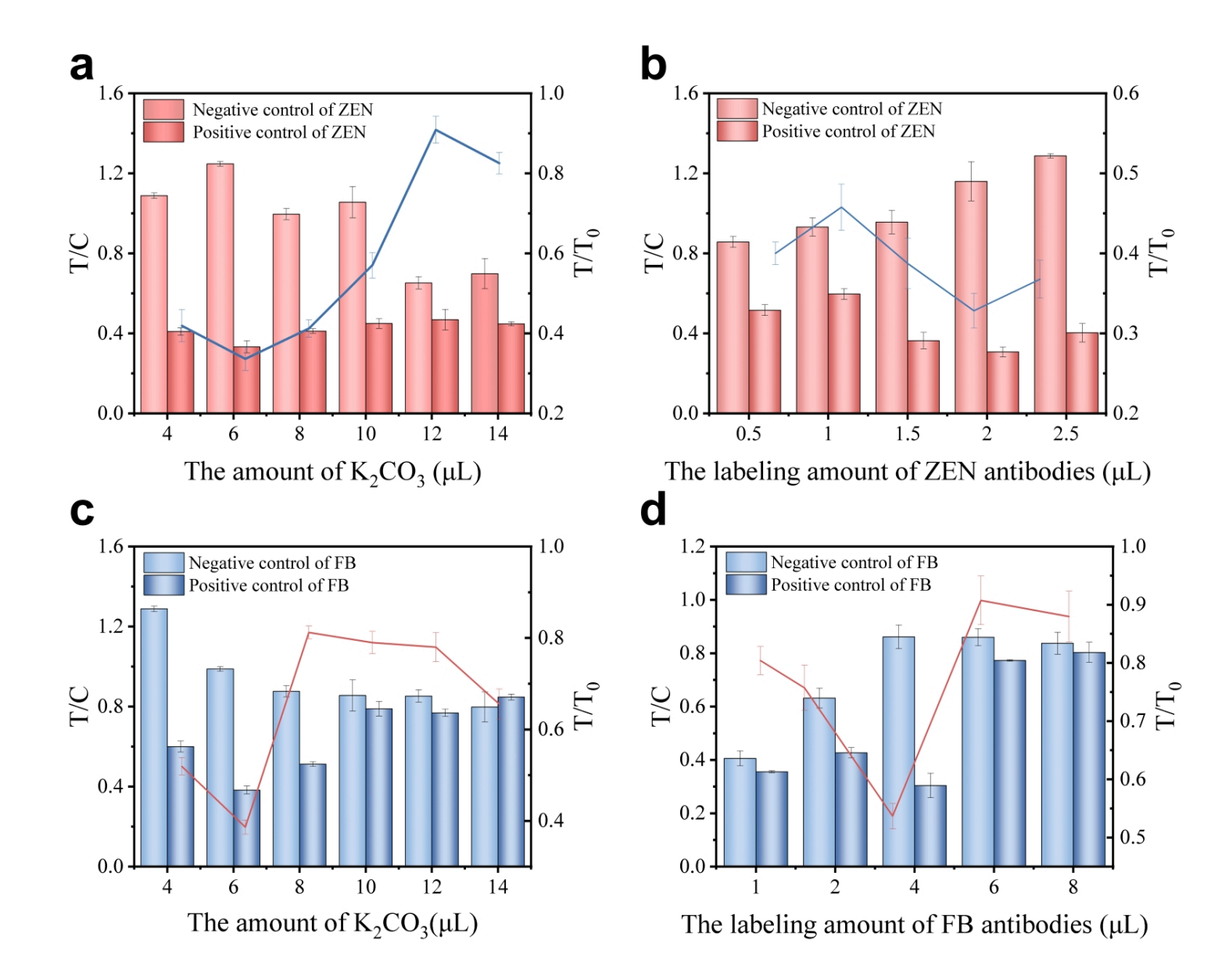
## **Figures**



Characterization of Zr-MOF@Pt. a: SEM image of Zr-MOFs; b: SEM image of MOF@Pt; c: TEM image of MOF@Pt; d: TEM elemental mapping of MOF@Pt; e: DLS analysis of MOF@Pt; f: Zeta potentials of MOF@Pt, MOF@Pt-AbZEN, and MOF@Pt-AbFB.



Schematic diagram of MOF@Pt-LFIA. a: Synthesis of Zr-MOFs@Pt; b: Assembly and advantages of MOF@Pt-LFIA; c: Detection principle of MOF@Pt-LFIA.



Optimization of K<sub>2</sub>CO<sub>3</sub> amount and antibody labeling amount for MOF@Pt antibody conjugation. a: Optimization of K<sub>2</sub>CO<sub>3</sub> amount for ZEN antibody conjugation with MOF@Pt; c: Optimization of K<sub>2</sub>CO<sub>3</sub> amount for FB antibody conjugation with MOF@Pt; b: Optimization of ZEN antibody labeling amount; d: Optimization of FB antibody labeling amount. The competitive inhibition rate is defined as  $(1-T/T_0)\times 100\%$ , where T and  $T_0$  represent the T line colorimetric

signal intensity values for positive and negative samples, respectively.

Figure 3

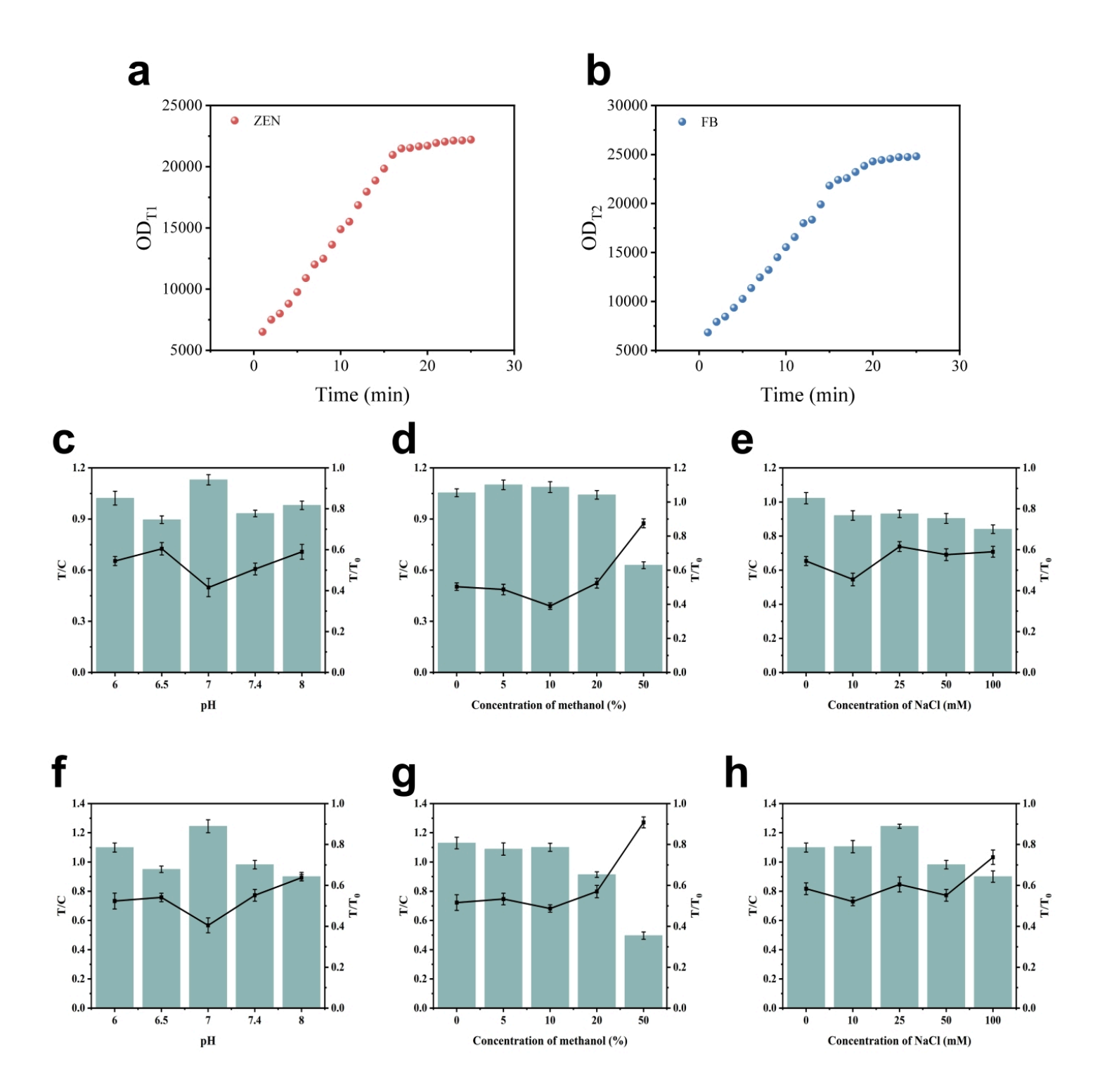


Figure 4

Optimization of detection conditions for the dual immunochromatographic assay strip. a, b: Kinetic curves of immune reaction time; c, f: pH optimization; d, g: Methanol concentration optimization; e, h: NaCl concentration optimization. The competitive inhibition rate is defined as  $(1-T/T_0)\times100\%$ , where T and  $T_0$  represent the T line colorimetric signal intensity values for positive and negative samples, respectively.

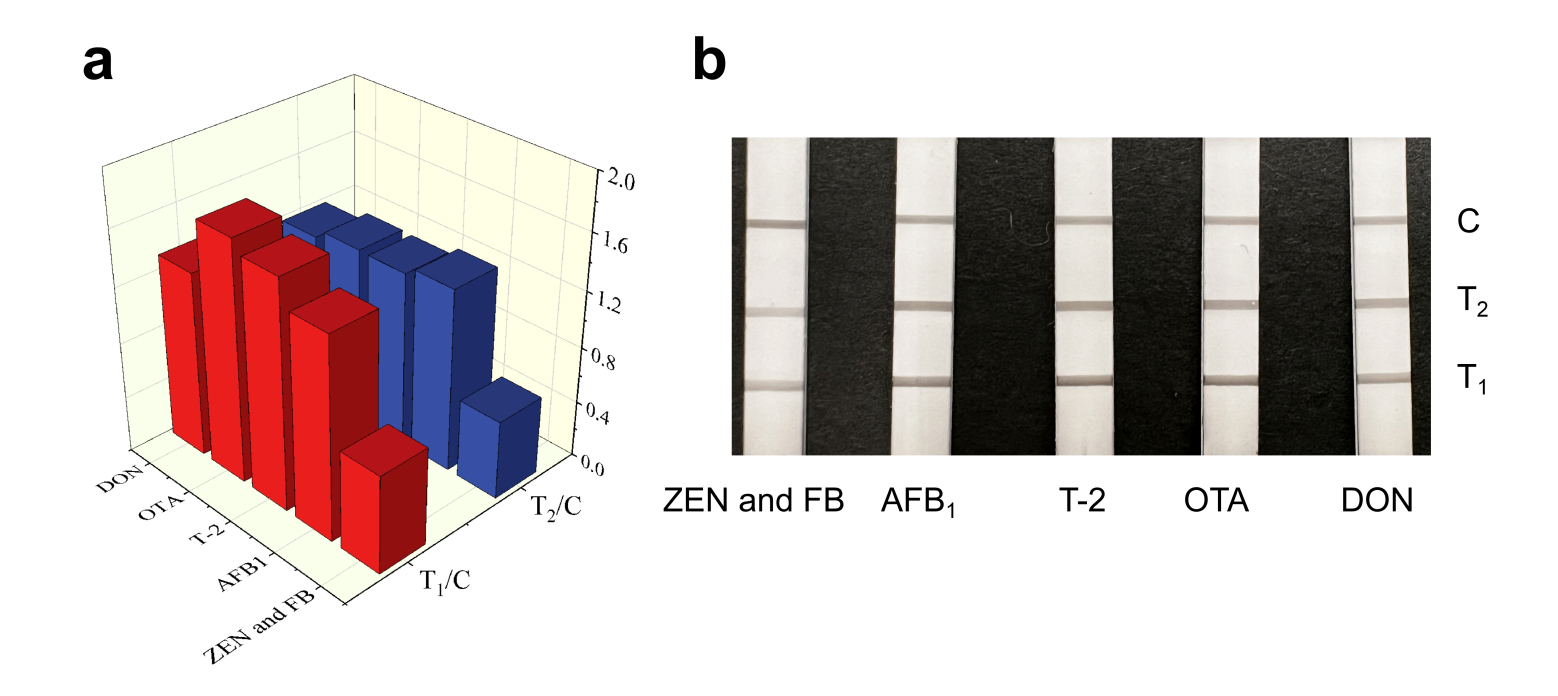


Figure 5

Specificity evaluation. a: MOF@Pt-LFIA specificity data display; b: MOF@Pt-LFIA specificity physical display.

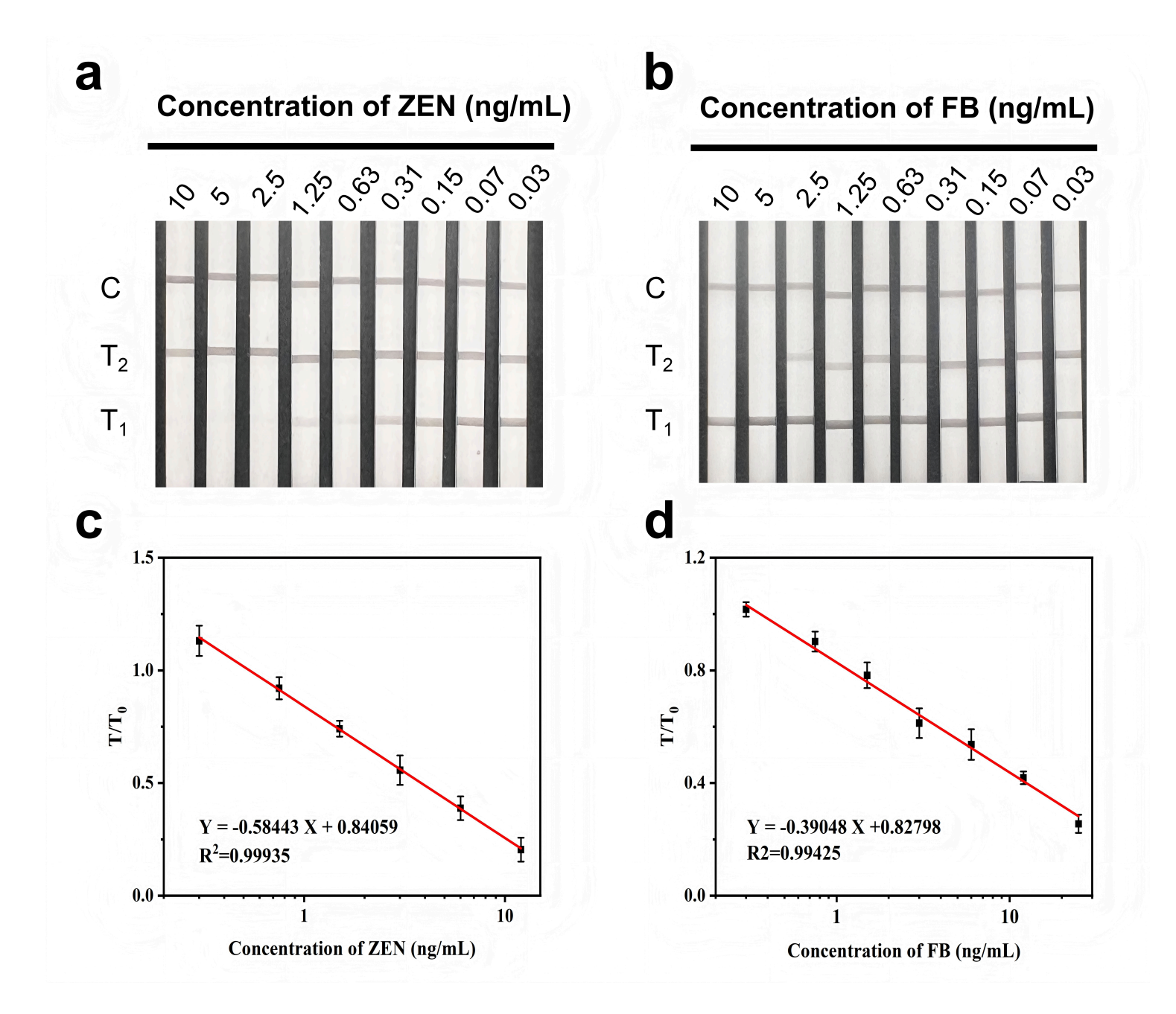


Figure 6

Real sample detection by MOF@Pt-LFIA. a, b: Physical images for detection of ZEN and FB; c, d: Standard curves for detection of ZEN and FB.

## **Supplementary Files**

This is a list of supplementary files associated with this preprint. Click to download.

GraphicAbstract.jpg